The survival of globular clusters in a cuspy Fornax

Shao, S.; Cautun, M.; Frenk, C.S.; Reina-Campos, M.; Deason, A.J.; Crain, R.A.; ... ; Pfeffer, J.

MNRAS 000, 1–15 (2020) Preprint 16 December 2020 Compiled using MNRAS LATEX style file v3.0

The survival of globular clusters in a cuspy Fornax

Shi Shao[1⋆], Marius Cautun[2,1], Carlos S. Frenk[1], Marta Reina-Campos[3,4,5], Alis J. Deason[1], Robert A. Crain[6], J. M. Diederik Kruijssen[3] and Joel Pfeffer[6]

[1] *Institute for Computational Cosmology, Department of Physics, Durham University, South Road Durham DH1 3LE, UK*
[2] *Leiden Observatory, Leiden University, PO Box 9513, NL-2300 RA Leiden, the Netherlands*
[3] *Astronomisches Rechen-Institut, Zentrum für Astronomie der Universität Heidelberg, Mönchhofstrasse 12-14, D-69120 Heidelberg, Germany*
[4] *Department of Physics & Astronomy, McMaster University, 1280 Main Street West, Hamilton, ON, L8S 4M1, Canada*
[5] *Canadian Institute for Theoretical Astrophysics (CITA), University of Toronto, 60 St George St, Toronto, ON M5S 3H8, Canada*
[6] *Astrophysics Research Institute, Liverpool John Moores University, 146 Brownlow Hill, Liverpool L3 5RF, UK*

16 December 2020

ABSTRACT

It has long been argued that the radial distribution of globular clusters (GCs) in the Fornax dwarf galaxy requires its dark matter halo to have a core of size $\sim$ 1 kpc. We revisit this argument by investigating analogues of Fornax formed in E-MOSAICS, a cosmological hydrodynamical simulation that self-consistently follows the formation and evolution of GCs in the EAGLE galaxy formation model. In EAGLE, Fornax-mass haloes are cuspy and well described by the Navarro-Frenk-White profile. We post-process the E-MOSAICS to account for GC orbital decay by dynamical friction, which is not included in the original model. Dynamical friction causes 33 per cent of GCs with masses $M_{\rm GC} \geq 4 \times 10^4$ M$_\odot$ to sink to the centre of their host where they are tidally disrupted. Fornax has a total of five GCs, an exceptionally large number compared to other galaxies of similar stellar mass. In the simulations, we find that only 3 per cent of the Fornax analogues have five or more GCs, while 30 per cent have only one and 35 per cent have none. We find that GC systems in satellites are more centrally concentrated than in field dwarfs, and that those formed in situ (45 per cent) are more concentrated than those that were accreted. The survival probability of a GC increases rapidly with the radial distance at which it formed ($r_{\rm init}$): it is 37 per cent for GCs with $r_{\rm init} \leq 1$ kpc and 92 per cent for GCs with $r_{\rm init} \geq 1$ kpc. The present-day radial distribution of GCs in E-MOSAICS turns out to be indistinguishable from that in Fornax, demonstrating that, contrary to claims in the literature, the presence of five GCs in the central kiloparsec of Fornax does not exclude a cuspy DM halo.

Key words: globular clusters: general – galaxies: dwarfs – methods: numerical

1 INTRODUCTION

One of the fundamental predictions of the standard cosmological model (ΛCDM) is that the density profiles of dark matter (DM) haloes have cuspy profiles of the Navarro-Frenk-White (NFW) form, where the inner DM density profile follows $\rho \propto r^{-1}$ (Navarro et al. 1996b, 1997). In contrast, some studies of stellar motions and rotation curves of faint galaxies often appear to indicate constant-density profiles at the centre, $\rho \propto r^0$ (e.g. Moore 1994; Flores & Primack 1994; Battaglia et al. 2008; Walker & Peñarrubia 2011). The apparent discrepancy between theoretical predictions and observations has become known as the core-cusp problem and several hypotheses have been proposed to explain it. These include modifications of the assumed nature of DM (e.g. Spergel & Steinhardt 2000; Rocha et al. 2013; Shao et al. 2013; Kaplinghat et al. 2016; Schneider et al. 2017), galaxy formation processes that alter the structure of the halo, (e.g. Navarro et al. 1996a; Read & Gilmore 2005; Pontzen & Governato 2012; Di Cintio et al. 2014; Benítez-Llambay et al. 2019), and systematic biases in the interpretation of the observational data (e.g. Oman et al. 2019).

Dwarf galaxies are important cosmological probes since their inner structure is particularly sensitive to the nature of DM; this has served to stimulate numerous studies of the rotation curve and kinematics of dwarfs. The kinematics of stars are tracers of the potential and multiple analysis methods have been employed to infer the mass profile of the DM halo in which they orbit, such as Jeans, and more complex, modelling (e.g. Gilmore et al. 2007; Walker et al. 2009; Amorisco et al. 2013; Pascale et al. 2018; Read et al. 2019). However, due to the relatively low number of stars with precise radial velocities measurements and the lack of accurate proper

⋆ E-mail: shi.shao@durham.ac.uk

motion measurements, the current data are unable to distinguish robustly between halo profiles with central cores or cusps in dwarfs (e.g. Strigari et al. 2010, 2017; Genina et al. 2018, 2019a). Dwarfs contains not only stars but many of them also host globular clusters (GCs) (e.g. Mackey & Gilmore 2003; Law & Majewski 2010; McConnachie 2012; Forbes et al. 2018), and these can also be used to constrain the profile of DM haloes.

Even though the scatter in the number of GCs associated with dwarf galaxies is large (e.g. Forbes et al. 2018), their presence in dwarf spheroidals like Fornax has long been considered a useful probe of the DM distribution in these galaxies. In particular, the GC system in Fornax has received considerable attention. It consists of five GCs that are found at an average projected distance of ~ 1.1 kpc from the centre (Mackey & Gilmore 2003). They are typically very old, with a lookback formation time, $t_{\rm age} \approx 12$ Gyrs (Fornax 4 is an exception with $t_{\rm age} \approx 10$ Gyrs; see Table 1). The interest in the Fornax GCs stems from comparing their ages to the orbital decay times (the time required for the GC to sink to the centre) due to dynamical friction. If the GCs formed at their present-day positions, then the orbital decay time in a cuspy DM halo would be shorter than their present age (e.g. Hernandez & Gilmore 1998; Goerdt et al. 2006); this discrepancy has been called the "GC timing problem". One simple solution is to increase the decay timescales by assuming larger initial radii for the GCs rather than assuming that they formed at their present-day positions (e.g. Angus & Diaferio 2009; Boldrini et al. 2019; Meadows et al. 2020). However, the initial positions where the GCs were born are difficult to constrain due to the long timescales involved.

An alternative solution is to assume that the inner density profile of the Fornax halo has a kiloparsec-sized core. Goerdt et al. (2006) used idealized N-body simulations to investigate the orbits of GCs under different assumptions for the DM profile. They argued that when dynamical friction is taken into account, the GCs would sink in a halo with a flat inner density profile and stall at some radius for a few gigayears. In contrast, in a cuspy halo, the GCs would gradually sink all the way to the centre and be disrupted quickly by the central tidal field or perhaps end up as a nuclear star cluster (e.g. Tremaine et al. 1975). Cole et al. (2012) also reported that if the core is relatively large, GCs could be pushed out by the so-called "dynamical buoyancy" mechanism. Based on the argument that GCs would stall in a halo with a central core, several studies have estimated the core radius of Fornax from the present-day positions of its GCs (e.g. Read et al. 2006; Inoue 2009; Cole et al. 2012; Petts et al. 2015; Kaur & Sridhar 2018; Boldrini et al. 2019).

Another possibility has been proposed by Boldrini et al. (2020) who have shown that if the GCs are surrounded by their own DM minihaloes, then there is no "GC timing problem" even in cuspy haloes. Finally, it is worth mentioning that tidal streams produced by the disruption of GCs stripped from dwarf galaxies can perhaps be used to distinguish between a central cusp or a core in the halo of the dwarf from which the GC was stripped (Malhan et al. 2020).

In this paper, we investigate if the present-day number and radial distribution of the GCs in the Fornax dSph are consistent with ΛCDM predictions in a cuspy DM halo. For this, we use one of the E-MOSAICS simulations that self-consistently model galaxy and GC formation and evolution in a fully cosmological context (Pfeffer et al. 2018; Kruijssen et al. 2019a). The presence of GCs does not affect the DM halo profile and so the E-MOSAICS dwarfs have the same DM profiles as in the EAGLE simulation, namely they are cuspy and well fitted by the NFW parametrisation (e.g. Schaller et al. 2015; Benítez-Llambay et al. 2019; Bose et al. 2019).

Table 1. Selected properties of the Fornax GCs. The columns give: GC designation, projected distance from the centre of the Fornax dSph, stellar mass, age and metallicity. The projected distances are taken from Mackey & Gilmore (2003) and updated for the current distance of the Fornax dSph of 147 kpc (McConnachie 2012). The remaining properties are taken from de Boer & Fraser (2016).

Name	r_p [kpc]	$M_{\rm GC}$ [10^5 $M_\odot$]	Age [Gyrs]	[Fe/H]
Fornax 1	1.72	0.42±0.10	12.1±0.8	-2.5±0.3
Fornax 2	1.13	1.54±0.28	12.2±1.0	-2.5±0.3
Fornax 3	0.46	4.98±0.84	12.3±1.4	-2.5±0.2
Fornax 4	0.26	0.76±0.15	10.2±1.2	-1.2±0.2
Fornax 5	1.54	1.86±0.24	11.5±1.5	-1.7±0.3
Fornax 6†	0.030	~ 0.29	–	–

† This is a recently discovered faint and highly elliptical GC, which is possibly undergoing tidal disruption (Wang et al. 2019). We estimated its mass by assuming that it has the same mass-to-light ratio as Fornax 1, which is the Fornax GC with the closest V-band magnitude to Fornax 6.

We proceed by selecting a sample of Fornax analogues in E-MOSAICS, that is galaxies with similar stellar mass to the Fornax dSph, and identify the GCs associated to each analogue. We cannot directly use the number and positions of those GCs since E-MOSAICS does not include an accurate calculation of GC orbital decay due to dynamical friction. Instead we account for this effect in post-processing. Firstly we trace back the GCs to either their formation time (for in-situ GCs) or their accretion time (for accreted GCs). Then, starting from these initial positions and velocities, we follow the orbital decay of the GCs by fitting an NFW profile to the host halo and analytically integrating the orbits subject to dynamical friction down to the present day. We account for the tidal disruption of the GCs that sink to the centre of the host galaxy. Finally, we compare the resulting present-day population of GCs in the simulation against the distribution of GCs in the Fornax dSph.

This paper is organised as follows. In Section 2 we describe the E-MOSAICS simulations and, in Section 3, we introduce our Fornax analogue sample and examine the properties of their DM haloes and GCs. In Section 4 we describe our method for modelling dynamical friction and tidal disruption of the GCs. In Section 5 we present our results on the number and radial distribution of GCs in Fornax-mass dwarfs. We conclude with a discussion of our results in Section 6 and a short summary of our main findings in Section 7.

2 SIMULATIONS

The E-MOSAICS (MOdelling Star cluster population Assembly In Cosmological Simulations within EAGLE) suite of cosmological hydrodynamical simulations is an extension of the 'Evolution and Assembly of GaLaxies and their Environments' (EAGLE) simulations (Crain et al. 2015; Schaye et al. 2015) that includes a subgrid model of stellar cluster formation, evolution, and disruption (Kruijssen et al. 2011; Pfeffer et al. 2018). For a detailed description of the physical ingredients of the model, we refer the reader to (Pfeffer et al. 2018; Kruijssen et al. 2019a).

Currently, the E-MOSAICS project consists of two groups of simulations. The first is a suite of 25 cosmological "zoom" simulations of MW-mass haloes (Pfeffer et al. 2018; Kruijssen et al.

2019a). These contain only a small number of Fornax analogues and are not used in this analysis. The second group, which is the one we use, is a simulation of a full cosmological volume in a periodic cube of side-length 34.4 (comoving) Mpc (Crain et al. in prep.). The volume of the simulation is 2.6 times larger than the EAGLE "high-resolution" simulation which has the same resolution (labelled Recal-L025N0752). The simulation follows the evolution of 1034^3 DM particles and an initially equal number of gas particles. The DM particle mass is 1.2×10^6 $\mathrm{M}_\odot$, and the initial gas particle mass is 2.3×10^5 $\mathrm{M}_\odot$. E-MOSAICS assumes the *Planck-1* cosmology (Planck Collaboration XVI 2014) with cosmological parameters: $\Omega_\mathrm{m} = 0.307, \Omega_\mathrm{b} = 0.04825, \Omega_\Lambda = 0.693, h = 0.6777, \sigma_8 = 0.8288$ and $n_\mathrm{s} = 0.9611$, which are those used by the EAGLE project.

As in the EAGLE project, the simulation we analyze here was performed with a modified version of the GADGET code (Springel 2005), which includes state-of-the-art smoothed particle hydrodynamics (Dalla Vecchia & Schaye 2012; Hopkins 2013; Schaller et al. 2015) and subgrid models, such as element-by-element gas cooling, star formation, metal production, stellar winds, and stellar and black hole feedback (Wiersma et al. 2009; Springel et al. 2005; Booth & Schaye 2009; Schaye et al. 2015). The parameters were calibrated so as to reproduce three present-day observables: the stellar mass function, the galaxy size–mass relation and the normalization of the relation between the masses of supermassive black holes and the stellar mass of their host galaxies. For a more detailed description we refer the reader to Schaye et al. (2015).

The semi-analytic model for MOSAICS was coupled with EAGLE to track the formation and evolution of star clusters. The model is calculated on-the-fly within EAGLE since the time resolution required to resolve the rapid change of the tidal field experienced by the GCs (< 1 Myr), which drives most of their disruption, is much finer than the time interval between simulation snapshots (roughly 70 Myrs). The formation of stellar particles in the simulation triggers the formation of a subgrid population of star clusters which inherit properties of their host stellar particles such as position, velocity, age, and metallicity.

The number of star clusters and their masses at formation are determined by two parameters, the cluster formation efficiency (CFE, Bastian 2008) and an upper truncation mass scale in the Schechter (1976) initial cluster mass function ($M_{c,\star}$), with a power-law index of -2 at low masses. These parameters are described in terms of the local natal properties of the GC, such as local ambient gas properties (pressure, density and mass) and stellar velocity dispersion. Environments with higher gas pressure lead to the formation of more star clusters which can also be more massive (Kruijssen 2012; Reina-Campos & Kruijssen 2017).

Four GC models are applied to the simulation in parallel. The fiducial model allows the CFE and $M_{c,\star}$ to vary as a function of properties of the local environment in which the stars are formed (Kruijssen 2012; Reina-Campos & Kruijssen 2017). The other three keep either, or both of the CFE and $M_{c,\star}$ fixed. For more details of the cluster formation models, we refer the reader to Pfeffer et al. (2018) and Reina-Campos et al. (2019). After the clusters form, they lose mass due to stellar evolution (according to the fractional mass-loss of the parent stellar particle) and by dynamical effects such as two-body relaxation and tidal shocks which are based on the strength and change of the local tidal field respectively (Kruijssen et al. 2011).

The E-MOSAICS simulations have been able to reproduce a broad range of observational properties such as the deficit of massive metal-poor GCs (i.e. the "blue tilt") in galaxies across a wide range of environments (Usher et al. 2018) and the diversity of age-metallicity relations of GCs in different galaxies (Kruijssen et al. 2019a). The $M_\mathrm{GC}/M_\mathrm{halo}$ and $M_\mathrm{GC}/M_\star$ relations predicted by the simulation are also in good agreement with observations (Bastian et al. 2020). Additionally, the large sample of MW-mass galaxies allows the assembly history of our MW and the GC formation history to be probed by reference to the observed present-day GC populations (Kruijssen et al. 2019b, 2020; Reina-Campos et al. 2019; Pfeffer et al. 2020; Trujillo-Gomez et al. 2020). The simulations also have strong implications for the origin of the stellar bulge and stellar halo whose masses are made up, in part, of GC remnants (Hughes et al. 2020; Reina-Campos et al. 2020). In addition, the simulations can be used to make predictions for the properties of the recently observed GCs in the M31 system (Hughes et al. 2019).

The halo and galaxy catalogues in E-MOSAICS have been built using the tools described by Schaye et al. (2015). Haloes are initially identified by the friends-of-friends (FOF) algorithm (Davis et al. 1985) with a linking length 0.2 times the mean interparticle separation. The resulting FOF groups are further split into gravitationally bound substructures using the SUBFIND code (Springel et al. 2001; Dolag et al. 2009), applied to the total matter distribution (dark matter, gas and stars) associated with each FOF group. The central subhalo is defined as the subhalo that contains the most bound particle, while the remaining subhaloes are classified as satellites. The stellar distribution associated with the main subhalo is identified as the central galaxy. The central haloes are characterized by the mass, M_{200}, and radius, R_{200}, that define an enclosed spherical overdensity of 200 times the critical density. The position of each galaxy, for both centrals and satellites, is given by their most bound particle.

Fig. 1 shows the relation between the stellar mass of central galaxies and the mass of their host haloes in E-MOSAICS. The satellite galaxies are not shown since the total mass associated with the subhalo changes as it orbits in the main halo. The scatter in the stellar-to-halo mass relation for Fornax-mass dwarfs is larger than for more massive galaxies, but is significantly smaller than for lower mass dwarfs (Sawala et al. 2015).

3 SAMPLE SELECTION AND METHODS

3.1 The Fornax analogue sample selection and their DM halo properties

We select Fornax analogues, to which we also refer as Fornax-mass dwarfs, in the simulation by requiring that they have a stellar mass in the range, $M_\star \in [2, 8] \times 10^7$ $\mathrm{M}_\odot$. This results in 1154 objects, of which 599 are field galaxies and 555 are satellites. The mass range used for the selection corresponds to a factor of two variation around the Fornax dSph stellar mass, which we take to be 4×10^7 $\mathrm{M}_\odot$ (de Boer et al. 2012). The mass range is relatively wide since we need a large sample of Fornax-mass dwarfs for good statistics and a factor of 2 is representative of the uncertainty in Fornax's mass estimates. A typical Fornax-mass dwarf in E-MOSAICS is resolved with $\sim2 \times 10^4$ DM particles, and hundreds of star particles, which allows for a robust determination of its present day properties as well as its formation history.

We study the general properties, such as halo mass, concentration, and scale radius, R_s, of the Fornax-mass dwarf sample in Fig. 2. The left panel shows the distribution of the host halo mass, M_{200}, for the field Fornax-mass dwarfs. The satellites are not shown since they are tidally stripped by the hosts after their infall. Nevertheless, for satellite dwarfs, we refer to the M_{200} of their

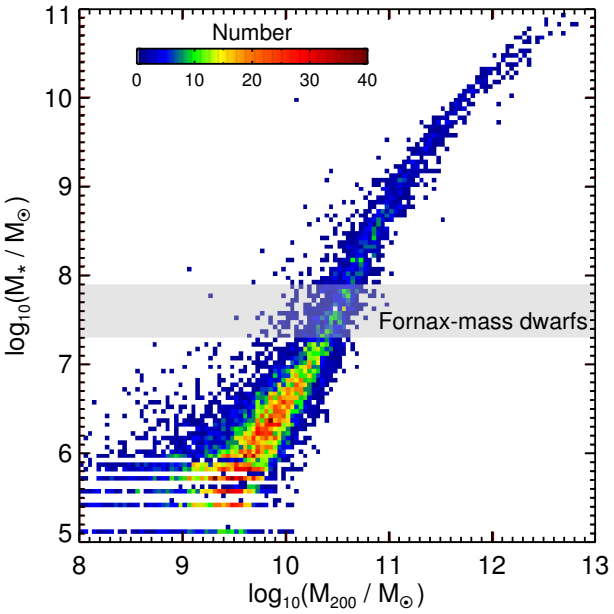

Figure 1. The relation between stellar mass, $M_\star$, and total halo mass, M_{200}, for central galaxies in the simulation. The colours indicate the number of galaxies in each halo and stellar mass bin (see legend). The grey shaded region shows galaxies with stellar masses in the range $2 - 8 \times 10^7$ $\mathrm{M}_\odot$, which corresponds to our sample of field Fornax-mass dwarfs (we also select Fornax-mass satellites, which are not shown in this diagram).

main progenitors, before they became a satellite of a more massive host, as their host halo mass. The distribution for the field sample peaks at a value of $2.8^{+1.1}_{-1.0} \times 10^{10}$ $\mathrm{M}_\odot$ (68 per cent confidence limit), with sharp drop-offs on both sides; this is in agreement with abundance matching predictions and results from other hydrodynamical simulations (e.g. Moster et al. 2013; Sawala et al. 2015; Oñorbe et al. 2015). The width of the distribution largely reflects the fact that haloes of a given mass can have a range of different concentrations; higher concentration haloes, which typically form early, have more time to form stars and experience less efficient feedback.

The concentration and scale radius of the host haloes are calculated by fitting the spherical DM density within a radial distance of 50 kpc from the centre (roughly the median R_{200} of the field Fornax-mass haloes) to an NFW profile (Navarro et al. 1996b, 1997):

$$\rho(r) = \frac{\rho_0}{\frac{r}{r_\mathrm{s}}\left(1 + \frac{r}{r_\mathrm{s}}\right)^2}\,, \qquad (1)$$

where ρ_0 and the scale radius, r_s, are parameters (see appendix A). For the satellites, we fit the DM profile of the main progenitor just before infall. The concentration is given by the ratio $c = r_\mathrm{s}/R_{200}$. The distribution of concentration values is shown in the middle panel of Fig. 2; it has a median value of $c = 10.5$ for the field Fornax-mass dwarfs. The result is in good agreement with previous high-resolution cosmological simulations (e.g. Hellwing et al. 2016).

The right panel of Fig. 2 shows the distribution of the scale radius, r_s, for both the field and satellite samples. The field sample has a median value of $r_\mathrm{s} = 6.2$ kpc, slightly larger than that of the satellite sample, $r_\mathrm{s} = 5.9$ kpc. The two samples have similar $z = 0$ stellar mass by construction; thus the difference in r_s between the two samples is due to satellites having experienced tidal stripping and also, potentially, to small differences in the assembly history of satellite versus central galaxies.

3.2 GCs sample selection and their formation time

Here we compare the E-MOSAICS predictions with the five most massive GCs in the Fornax dSph. These have been known for a long time and have been thoroughly studied (e.g. de Boer & Fraser 2016); we give a few selected properties of the Fornax GCs in Table 1. More recently, Wang et al. (2019) discovered a sixth GC in Fornax. It has a lower mass than the other five and is possibly undergoing tidal disruption. For simplicity, and better to compare with previous works, we limit our comparison to the five well-known Fornax GCs.

To identify analogues of the Fornax GC population, we proceed by selecting all GCs that at $z = 0$ are associated with a Fornax analogue and have a stellar mass above 4×10^4 $\mathrm{M}_\odot$. The GC stellar mass threshold corresponds to the mass of the Fornax-1 GC, the least massive of the five Fornax GCs we study here. Our selection results in 2133 GCs, out of which only 1439 survive to the present day (the others were tidally disrupted after dynamical friction dragged them to the centre – we describe this in detail in Section 4.1).

GCs that are associated with their $z = 0$ host may have formed inside another galaxy that was subsequently accreted into the present-day host. Such GCs can have different properties (e.g. age, metallicity, radial distribution) from those born *in situ*. We study this by splitting our sample into *in situ* and accreted GCs according to whether they were formed in the main (*in situ*) or in a sub- (accreted) branch of the progenitor of the $z = 0$ host galaxy of each GC. We find that around half (45 per cent) of the GCs formed *in situ*.

Fig. 3 shows the probability distribution function (PDF) of GC formation times for both *in situ* and accreted objects that survive to $z = 0$. Overall, GCs in E-MOSAICS have very early formation times, with more than half of the full sample having formed within the first 2 Gyrs after the Big Bang; this is consistent with the inferred ages of the GCs in Fornax. The only exception is Fornax 4 which is $\sim$ 10 Gyrs old and is relatively 'younger' than the other four GCs, as indicated by its more metal-rich stellar population (de Boer & Fraser 2016).

More interestingly, when comparing the accreted and *in situ* GC populations, we find that 77 per cent of accreted GCs formed early ($\sim$ 12 Gyrs old), while this fraction is only 23 per cent for the *in situ* ones. The variation in formation times between the two GC populations is expected, since there are at least two processes that act differently in the two populations. The accreted population is brought in by mergers, and most such mergers take place at $z \gtrsim 2$; by construction, those GCs must have formed before the merger. Secondly, as we shall discuss later, *in situ* GCs are more radially concentrated and thus dynamical friction is more efficient at causing them migrate to the centre, where they are tidally disrupted. This would suggest that recently formed *in situ* GCs are more likely to survive to $z = 0$ than their older siblings. Both of these processes lead to an excess of younger *in situ* GCs.

It is also worth noting that Fornax has two or more distinctive populations of stars: a metal poor and a younger, more compact, metal rich population (e.g. Battaglia et al. 2006). One way to obtain such configurations in simulations is through a major merger between two dwarfs (e.g. Benítez-Llambay et al. 2016; Genina et al.

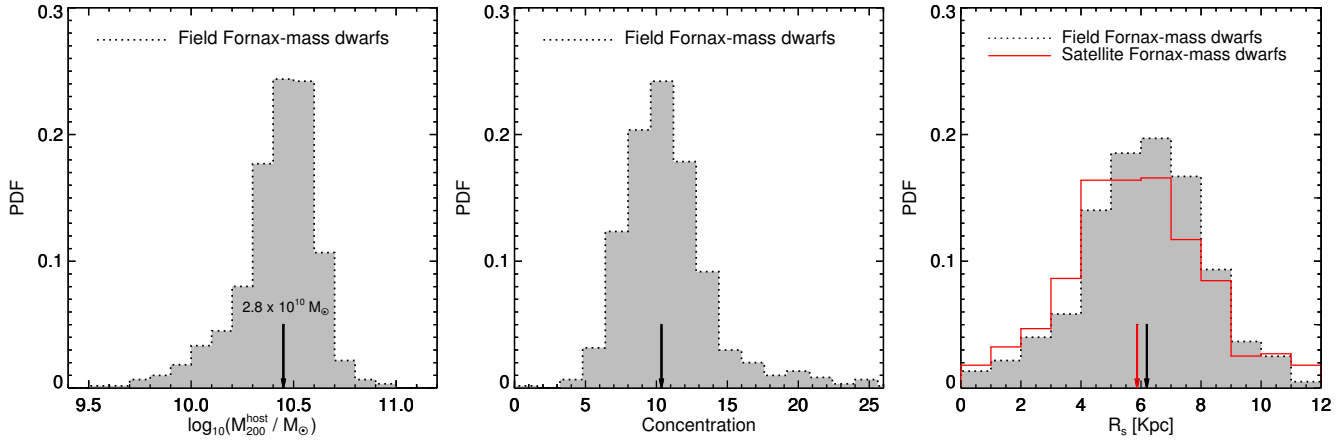

Figure 2. The properties of the DM haloes that host a Fornax-mass dwarf galaxy. The plot shows the PDF of the halo mass (left panel), concentration (centre panel), and scale radius (right panel). The results are for present-day field galaxies, since the same properties for satellite galaxies are not directly comparable (see text for discussion on this). However, we do show the distribution of scale radii for satellites as the solid red line in the right panel. The vertical arrows indicate the median of each PDF.

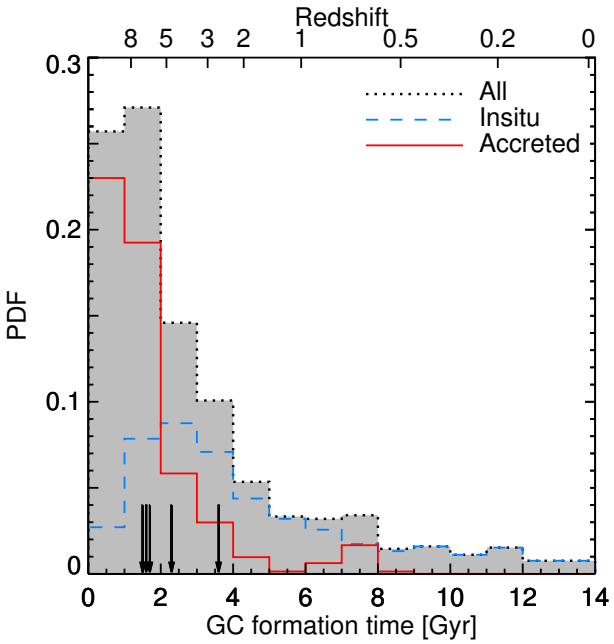

Figure 3. The distribution of formation times for GCs found in Fornax-mass dwarfs at $z = 0$. The plot shows the PDF for all GCs (black dotted line), *in situ* (blue dashed line) and accreted (red solid line) GCs. Arrows indicate the formation time of Fornax's GCs (de Boer & Fraser 2016). The left-hand side of the plot corresponds to the Big Bang and $t = 13.8$ Gyrs to present day.

2019b), raising the intriguing possibility that Fornax might have had one or more such mergers (see also Yozin & Bekki 2012).

4 GC ORBITAL EVOLUTION

In the E-MOSAICS model GCs are associated with stellar particles whose dynamics they follow. Like the stars, GCs are collisionless objects and thus this is a reasonable approximation, except for one aspect: GCs can experience significant dynamical friction as they orbit in their host galaxy. This process is central to this study and thus we need to supplement the E-MOSAICS model with a treatment of dynamical friction. We do this by post-processing the simulated GC populations from E-MOSAICS as follows. We trace back each GC associated with a present-day Fornax analogue to the simulation snapshot closest to the time when the GC formed (for *in situ* objects) or to the time when it was accreted into its $z = 0$ host (for accreted GCs). The corresponding positions and velocities, which are given by E-MOSAICS, are taken as the starting position of each GC and its orbit is modelled in the potential of its host galaxy accounting for dynamical friction. Finally, we follow the orbit of each GC until the present day keeping track of whether it got close enough to the galaxy centre to experience tidal disruption. In this section, we present the model used to follow the GC orbit evolution.

4.1 Dynamical friction

We follow the evolution of each GC separately in the potential of the DM halo and stellar component of its host galaxy. The DM halo is modelled as an analytic Navarro, Frenk & White (Navarro et al. 1996b, 1997, hereafter NFW) profile with total mass, M_{200}, and concentration, c, whose potential is given by:

$$\Phi_{\rm halo} = -\frac{GM_{200}}{r}\frac{\ln\left(1+r/r_{\rm s}\right)}{\ln(1+c)-c/(1+c)}\,, \qquad (2)$$

where $r_{\rm s}$ denotes the scale radius of the DM halo. The halo parameters, c, $r_{\rm s}$ and M_{200}, are inferred by fitting an NFW profile to the host DM halo at $z = 0$ for field Fornax-mass galaxies and at infall for the Fornax-mass galaxies that are satellites at the present day. In the latter case, we assume that the GC orbit is determined only by its Fornax-mass host, and we ignore additional forces coming from the more massive system to which the Fornax-mass satellite belongs. This approximation is valid as long as the inner region, $r \lesssim r_{\rm s}$, of the Fornax-mass satellite does not undergo severe tidal disruption.

The GC dynamics are dominated by the DM halo potential, but, for completeness, we also include the stellar potential. We model the stellar component of the Fornax-mass galaxy as a Plummer profile with potential:

$$\Phi_{\rm stars} = -\frac{GM_{\star}}{\sqrt{r^2+b^2}}\,, \qquad (3)$$

where $M_\star$ denotes the stellar mass and the parameter, b, is given by $b = R_{1/2}/1.3$, with $R_{1/2}$ the 3D stellar half-mass radius. The Plummer profile gives a good match to the stellar density profile of Fornax and other dwarf spheroidal galaxies around the Milky Way (e.g. see Wang et al. 2018).

We implement dynamical friction as a deceleration experienced by the GC while orbiting within the host halo of its galaxy. We assume that the deceleration is given by Chandrasekhar's formula,

$$\frac{\mathrm{d}\mathbf{v}}{\mathrm{d}t} = -\frac{4\pi G^2 M_{\rm GC}\rho \ln\Lambda}{v^2}\left[\mathrm{erf}(X) - \frac{2X}{\sqrt{\pi}}e^{-X^2}\right]\frac{\mathbf{v}}{v}\,, \quad (4)$$

(Binney & Tremaine 2008), where G is the gravitational constant, $M_{\rm GC}$ is the GC mass, $\mathbf{v}$ is the relative velocity of the GC with respect to its galaxy, ρ is the density of the DM halo at the GC's position, and $X = v/(\sqrt{2}\sigma_v)$, with σ_v the local 1D velocity dispersion of the DM halo. We take the Coulomb logarithm as:

$$\ln\Lambda = \ln\frac{b_{\rm max}\sigma_v^2}{GM_{\rm GC}}\,, \quad (5)$$

(Goerdt et al. 2006), where $b_{\rm max}$ is the largest impact parameter to be considered. By comparing with high resolution simulations of GC orbit evolution, Goerdt et al. (2006) found that for cuspy haloes, $b_{\rm max} = 0.25$ kpc is the best fitting value. We include only the dynamical friction arising from the DM halo, which is the dominant effect, and neglect any contribution from the stellar distribution.

When integrating the orbits of the GCs we keep the potential of the DM halo fixed at all times. This is a reasonable approximation since, while the halo mass can grow by factors of several since the time most GCs formed, ∼12 Gyrs ago, the growth takes place by adding new mass to the outskirts of the halo while leaving the inner region mostly unchanged (Wang et al. 2011). Most stars and GCs orbit in the inner few kiloparsecs of the halo and thus their orbits will not be affected by mass growth at the halo outskirts. However, this approximation ceases to be valid when a halo undergoes major mergers. In that case, the GC orbits can also be affected and, on average, they are pushed slightly towards higher energy and more extended orbits (e.g. Benítez-Llambay et al. 2016). This would reduce the effect of dynamical friction and slow down the orbital decay of GCs. Thus, by not accounting for the effect of major mergers, we are likely overestimating the number of GCs that sink to the centre of their host.

4.2 Tidal disruption of GCs

To account for the disruption of GCs by the tidal field of their host galaxy we calculate their tidal radius. For an NFW profile the tidal radius for a GC on a circular orbit at distance, r, from the galaxy centre is given by:

$$r_{\rm tidal} = (r + r_{\rm s})\left(\frac{M_{\rm GC}}{M_{200}}\frac{r}{3r + r_{\rm s}}\right)^{\frac{1}{3}}\,, \quad (6)$$

(Renaud et al. 2011; Orkney et al. 2019). This expression neglects the tides arising from the stellar distribution of the host galaxy, which are much smaller than the tidal field of the DM halo. We calculate the tidal radius at each point along the GC's orbit and consider the GC to be destroyed by the tidal field of its host when the tidal radius is comparable to the half-mass radius of the GC. As GCs lose mass due to two-body relaxation as well as tidal stripping, their half-mass radius increases. According to the N-body simulations of Orkney et al. (2019), GCs evolving in cuspy profiles can reach a half-mass radius of ∼6 pc, after which the mass loss rate increases rapidly and the GC is disrupted shortly thereafter. Based on these results, we assume that GCs are fully disrupted if at any point along their orbit the tidal radius becomes smaller than 6 pc.

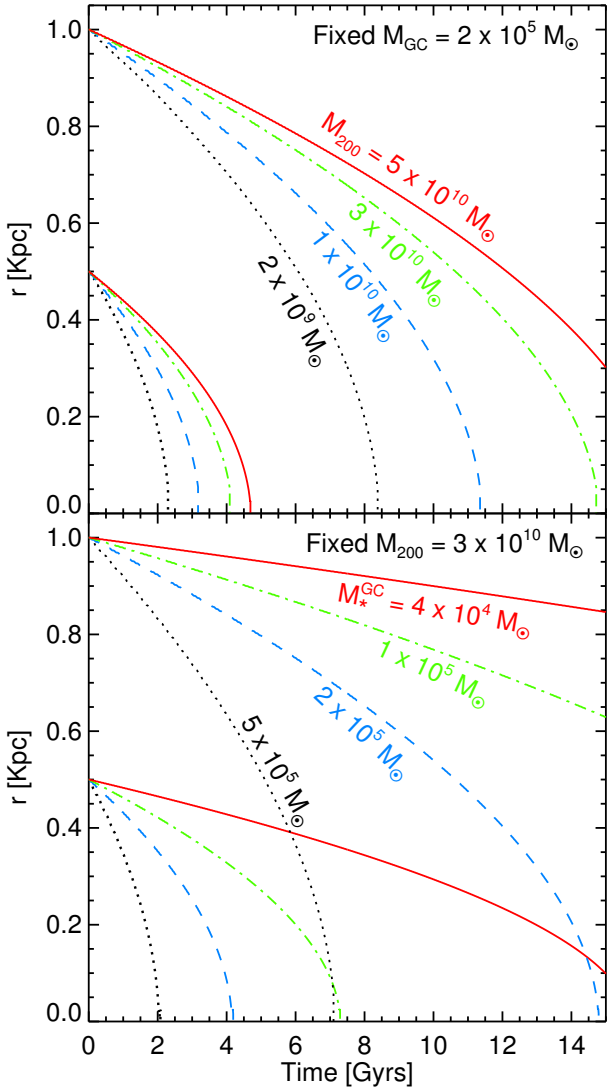

Figure 4. The time evolution of the radial distance for two GCs on circular orbits whose starting positions are at 0.5 kpc and 1 kpc from the centre of its host. The top panel shows how the orbits change when varying the host halo mass (here, the GCs have the same mass, $M_{\rm GC} = 2 \times 10^5$ M$_\odot$). The bottom panel shows how the orbits change when varying the GC mass (here, the host halo has the same mass, $M_{200} = 3 \times 10^{10}$ M$_\odot$).

4.3 Decay of the GC orbits

The orbital decay time of a GC is mainly determined by two factors: 1) the initial distance to the center of its host, and 2) the mass ratio between the GC and the host halo. We illustrate this in Fig. 4, where we show GC orbits for two starting positions and a selection of GC and host halo masses. In all cases, we start with GCs on circular orbits; in reality, E-MOSAICS predicts highly elliptical orbits even for the *in situ* GCs of our Fornax-analogue sample, with a median ellipticity at birth of 0.64 (and 16 to 84 per centile of the ellipticity distribution of 0.36 and 0.84 respectively). How-

ever, here we want to illustrate the systematic effect of dynamical friction, which is most clearly seen for circular orbits.

In the first example, in the top panel in Fig. 4, we fix the GC mass to $M_{\rm GC} = 2{\times}10^5$ M$_\odot$, which is the median mass of Fornax's GCs, and vary the mass of the host halo. We select a reference halo mass, $M_{200} = 3 \times 10^{10}$ M$_\odot$, which corresponds to the median halo mass in our Fornax analogue sample, as well as a much lower mass, $M_{200} = 2 \times 10^9$ M$_\odot$, which was the value used by Goerdt et al. (2006). We also present orbits for host halo masses $M_{200} = 1$ and 5×10^{10} M$_\odot$, which correspond to roughly the 10 and 90 per centile of the distribution of halo masses for our sample of Fornax-mass dwarfs.

We show the orbital evolution for two starting distances from the host centre: 0.5 kpc and 1 kpc. As expected, GCs that are initially closer to the centre sink more quickly than those which start further away. GCs with $r_{\rm init} = 0.5$ kpc sink to the center within $\sim$ 2 Gyr in the least massive halo ($M_{200} = 2 \times 10^9$ M$_\odot$), and $\sim$ 5 Gyr in the most massive host halo ($M_{200} = 5 \times 10^{10}$ M$_\odot$). The sinking time of GCs increases when increasing $r_{\rm init}$. For $r_{\rm init} = 1$ kpc, the GC can survive for a Hubble time in the two most massive hosts, but not in the lower mass haloes.

In view of the diversity of the mass of the Fornax GCs, in the bottom panel we study the variation in orbits with GC mass. In this case, we fix the halo mass to $M_{200} = 3 \times 10^{10}$ M$_\odot$, the median value for Fornax-mass hosts in the E-MOSAICS simulation (see Fig. 3). We show orbits for four GC masses, from 4 to $50{\times}10^4$ M$_\odot$. The lowest mass GC experiences the weakest orbital decay, and survives for a Hubble time even when starting at $r_{\rm init} = 0.5$ kpc. In contrast, the most massive GC sinks rapidly to the centre, with a sinking time of 2 and 7 Gyrs depending on whether it starts at 0.5 or 1 kpc from the centre. This suggests that the most massive GC in Fornax, Fornax-3, must have formed significantly farther than its present-day position (0.46 kpc projected distance); we discuss this point in greater detail in Sections 6 and in Fig. 10.

The oldest GCs can lose up to 60 per cent of their initial mass due to dynamical effects, such as two-body relaxation, tidal stripping and stellar evolution (see Appendix C). We account for this effect by having a time-varying mass for our GCs, with the mass decreasing in time according to the prescription detailed in Appendix C.

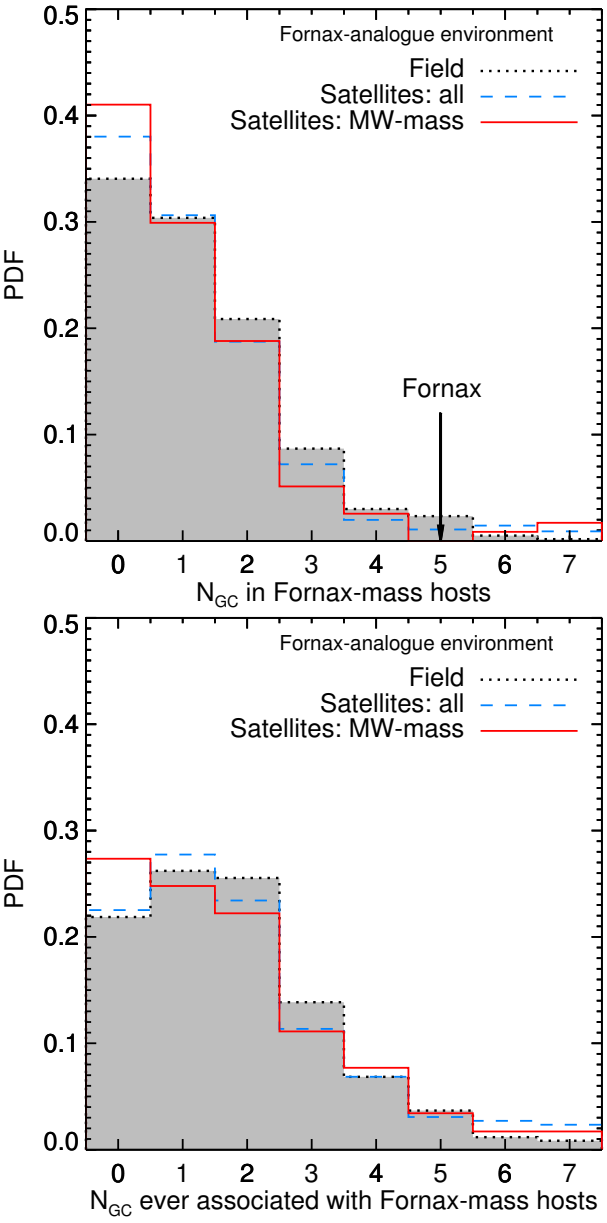

Figure 5. *Top panel*: PDF of the number of GCs at $z = 0$ in Fornax analogues. We only show GCs with present-day masses above $4{\times}10^4$ M$_\odot$, the lowest mass GC in Fornax. The three lines show the distribution for Fornax-mass dwarfs in the field (dotted line), for satellites around all hosts (dashed line) and for satellites around MW-mass hosts (solid line). *Bottom*: same as the top panel but counting also the GCs more massive than 4×10^4 M$_\odot$ that were tidally disrupted after sinking to the centre of their host galaxy.

5 RESULTS

We now compare the number and radial distribution of GCs in the Fornax dSph with the E-MOSAICS predictions. These predictions have been post-processed to include dynamical friction and exclude GCs that were tidally disrupted after sinking to the centre of their host, as described in the previous section.

5.1 The number of GCs in Fornax-mass dwarfs

The first question we address is how frequently do the simulations produce dwarfs with the number of GCs observed in the Fornax dSph, that is at least five with mass, $M_{\rm GC} > 4 \times 10^4$ M$_\odot$? We answer this question in the top panel of Fig. 5, which shows the distribution of the number of GCs that survive to $z = 0$ in our Fornax analogue sample. Regardless of whether they are satellites or field galaxies, nearly 35 per cent of the Fornax-mass hosts do not have any GCs at all and 30 per cent have only one object. Thus, E-MOSAICS predicts a low number of GCs in Fornax-mass dwarfs. Field dwarfs tend to have more GCs than satellite galaxies, but the effect is rather small. The difference could be due to: i) satellite dwarfs having stopped forming stars, and hence GCs, after falling into their host (although infall can lead to at least a temporary increase in star formation, e.g. Shao et al. 2018; Genina et al. 2019b; Hughes et al. 2019), and ii) having had some of the GCs that were on extended orbits tidally stripped by their more massive host.

When comparing with the Fornax dSph we find that only 3 per cent of the simulated analogues have five or more GCs. Thus, systems of GCs as rich as the one observed in Fornax are predicted to be rather rare. As we mentioned in the previous section, around 33 per cent of the GCs that formed within, or were accreted into,

our Fornax analogues sunk to the centre of these systems and were tidally destroyed. So, could the rarity of GC-rich dwarfs in our model be due to tidal destruction of GCs? We answer this question in the bottom panel of Fig. 5 where we again show the PDF of the GC count for each Fornax-mass dwarf, but now we include also the tidally destroyed GCs. Thus, the panel shows the E-MOSAICS prediction for the PDF of all the GCs that ever formed within, or fell into, a present-day Fornax-mass dwarf.

As expected, we find an increase in the number of GCs per dwarf galaxy. In particular, we find a decrease in the fraction of dwarfs with none or one GC, and an increase in systems with two or more GCs. However, the tail of the distribution corresponding to five or more GCs changes only slightly, with the chance of having a GC system as rich as the Fornax dSph increasing to only 6.5 per cent. This value is still rather low and indicates that the tidal destruction of GCs is not the main factor responsible for the low prevalence in E-MOSAICS of GC systems as rich as the one in Fornax. The main difference between haloes with a central core and those with a cusp is the fraction of tidally disrupted GCs, which is expected to be lower for the former case (e.g. Goerdt et al. 2006; Meadows et al. 2020). Thus, the number of Fornax GCs is not a reflection of whether or not the dark matter halo profile has a central core or cusp.

The number of GCs in a galaxy depends strongly on the mass cut used for the GC selection. Here, we only select GCs with a present-day stellar mass above 4×10^4 M$_\odot$, which is the mass of the lightest GC in Fornax. The uncertainty in the mass estimate of that GC is $\sim 1 \times 10^4$ M$_\odot$ (25 per cent fractional error), as shown in Table 1. To have a fair comparison between our model prediction and the data we should include this measurement error in our predictions. We recalculate the fraction of hosts that have five or more GCs by adding a random error to the GC mass, given by a Gaussian distribution with zero mean and standard deviation, 1×10^4 M$_\odot$. We find that the inclusion of errors leads to a small increase in the fraction of GC systems as rich as the one in Fornax. For our fiducial case that includes GC tidal disruption, the prevalence of Fornax GC systems grows from 3 per cent, when no mass error is included, to 4 per cent when modelling mass measurement errors.

The E-MOSAICS predictions have been shown to agree well with observational data (Kruijssen et al. 2019a) such as the total mass in GCs at a given host halo mass or host galaxy stellar mass (for details see Fig. 1 in Bastian et al. 2020). This suggests that the paucity of rich Fornax-like GC systems is unlikely to be due to a failure of the GC formation and evolution model and that, most likely, *suggests that Fornax has an excess of GCs for its stellar mass.*

A census of GCs in galaxies as faint as Fornax is currently lacking and the available observations are rather heterogeneous, which makes it difficult to perform a robust comparison between Fornax and other equal-mass dwarfs. However, from the currently available data in Forbes et al. (2018), which provides a table of all dwarf galaxies with one or more GCs, we conclude that our predictions in Fig. 5 are broadly consistent with observations. For example, the table of Forbes et al. contains 9 dwarfs with luminosity within ± 1 mag of the Fornax dSph. Of those, the majority (7 out of 9) have either one or two GCs, and only two systems, Fornax and UGC685, have more than two (interestingly, both these galaxies have 5 GCs).

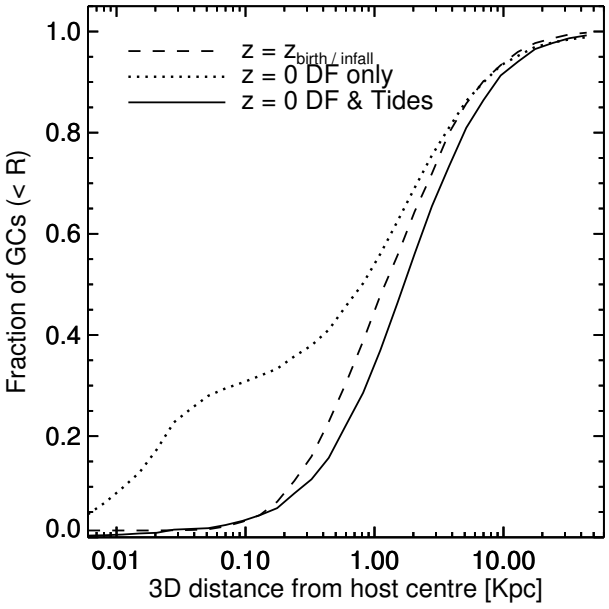

Figure 6. The 3D radial distribution of GCs in Fornax-mass dwarfs. The dashed line shows the distribution of GCs at birth, if they formed *in situ*, or at infall into their Fornax analogue host, if they were accreted. Dynamical friction leads to some GC sinking to the centre of their host and the resulting $z = 0$ distribution is shown by the dotted line. Once a GC gets close enough to the centre, it is disrupted by the tides of the host galaxy. The resulting $z = 0$ radial distribution is shown by the solid line and includes the effect of both dynamical friction and tidal disruption.

5.2 The radial distribution of GCs

Since, as we have seen, the high number of GCs in Fornax is not in itself a reliable way to infer if the DM halo is cuspy or has a core. In this section we examine the constraints that can be placed on the inner structure of Fornax by considering instead the radial distribution of its GCs. Most dwarfs have one or two GCs, so it is difficult and not very meaningful to show the radial distribution for each host. Instead, we stack all our Fornax-mass dwarfs and study the *mean* radial profile of GCs obtained by stacking the distances to their host's centre.

We start with Fig. 6 which shows how the 3D radial distribution of GCs changes from their initial position to the present day. The dashed line shows the initial positions of GCs which correspond to either their birth location (for *in situ* GCs) or to their position at the time they were accreted into their $z = 0$ host (for accreted GCs). There is a large range of initial positions, with a median value of 1.7 kpc and 10 and 90 per centiles of 0.3 and 8.5 kpc respectively. Although not shown, we have checked that the *in situ* population is more concentrated than the accreted sample.

The subsequent orbital evolution leads to the GCs moving inwards on average, as illustrated by the dotted line in Fig. 6, which shows the $z = 0$ positions after including the effect of dynamical friction but without removing tidally destroyed GCs. We find that around one third of the GC sample sinks to the centre of their galaxies, i.e. to $r < 0.1$ kpc, and thus are likely to be tidally disrupted. When accounting for tidal disruption, we find that the majority of GCs with $r \lesssim 0.2$ kpc are removed and the distribution of surviving GCs, which is shown by the solid line in Fig. 6, is now somewhat less concentrated than the initial GC positions.

In Fig. 7 we investigate if GC systems in all Fornax-mass dwarfs have the same average radial profile. In particular, we study

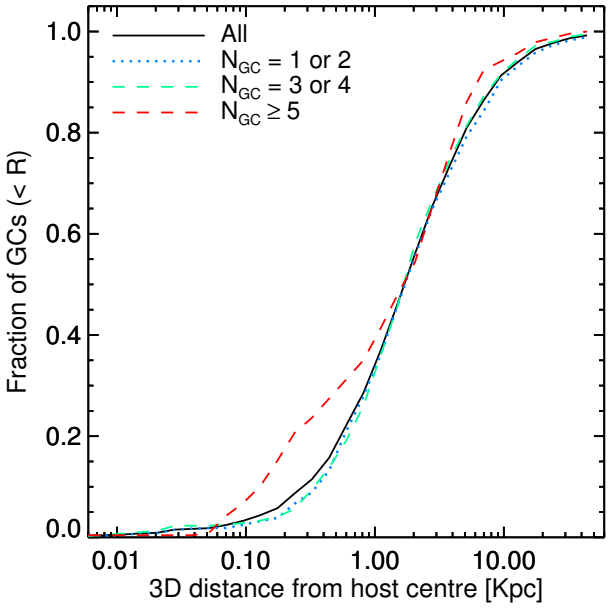

Figure 7. The dependence of the 3D radial distribution of GCs on the number of GCs in a Fornax-mass dwarf. It shows that there is no correlation between the radial distribution of GCs and the number of GCs in a galaxy.

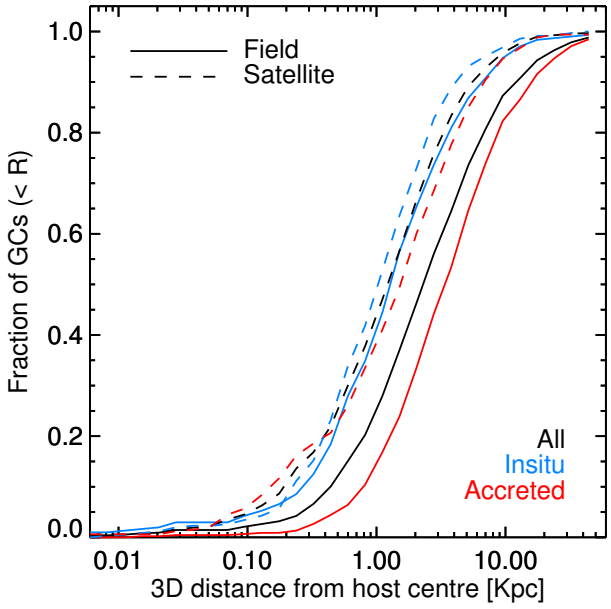

Figure 8. Comparison of the present-day radial distribution of GCs in field (solid lines) and satellite (dashed lines) Fornax-mass hosts. For each subsample we show the distribution of all GCs (in black), those formed *in situ* (in blue) and those accreted (in red).

if the radial profile depends on the number of GCs in a given galaxy. This test is motivated by our previous result that Fornax has a large number of GCs for its stellar mass and we wish to investigate if such an excess also impacts the GC radial distribution. The figure shows that there is no significant correlation between the number of GCs and their radial distribution. (While the dashed line shows some deviations from the mean trend, these are consistent with random scatter given the small sample size.) In practice, this shows that no systematic bias is introduced when comparing the Fornax GC distribution with the average profile of the full Fornax analogue sample.

Fig. 8 investigates how the radial distribution of GCs differs in satellite and field dwarfs. GCs in satellite dwarfs (black-dashed line) are more radially concentrated than those in field dwarfs (black-solid line): nearly half of the GCs in satellites are located within 1 kpc from the centre while only 25 per cent in the field dwarfs are. The difference between satellite and field dwarfs is due to tidal stripping of GCs in satellite dwarfs, which preferentially removes objects on extended orbits and thus leads to more concentrated distributions. While not shown, we have checked this by tracing back the satellite and field dwarfs to redshift, $z = 2$, and comparing their GC distributions at that time. To make a meaningful comparison, for the $z = 0$ satellites, we used only the $z = 2$ progenitors that were central galaxies, which represent the bulk of the population. We find that at redshift $z = 2$ there is no significant difference in the GC distributions of progenitors of satellite and field dwarfs. Thus, the differences seen in Fig. 8 are mainly due to tidal stripping from the outskirts of satellite dwarfs.

In Fig. 8 we further split the GCs into two additional subsamples: accreted and *in situ*. In both satellite and field Fornax analogues, the *in situ* GCs are more radially concentrated than the accreted population. The segregation between the *in situ* and accreted components is largest for field dwarfs. The fraction of accreted GCs in satellite dwarfs is 50 per cent, lower that the 60 per cent fraction in field dwarfs. This difference could be due to two effects. First, satellite galaxies experience mergers mostly before infall into a more massive host halo (see e.g. Angulo et al. 2009; Deason et al. 2014); they thus have less time to devour other galaxies and grow their accreted GC population. Secondly, as we have just seen, accreted GCs have a more radially-extended distribution than the *in situ* GCs and so they are more easily tidally stripped from their hosts.

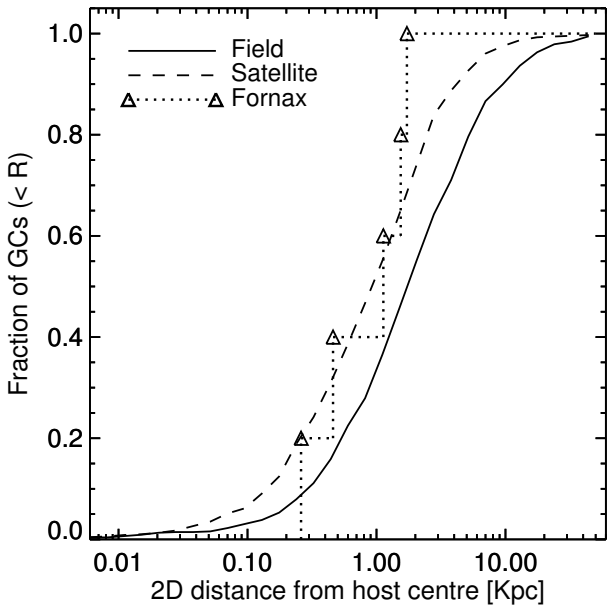

Figure 9. The distribution of projected 2D distances of GCs in Fornax analogues. The solid and dashed lines show the results for respectively field and satellite Fornax-mass dwarfs. The observed projected distances of GCs in Fornax are shown by the dotted line (each triangle symbol corresponds to a Fornax GC). The distribution of GCs in Fornax matches very well that of its analogues in the simulation.

Finally, we compare the GC radial distribution of our Fornax analogues with that of the real Fornax dSph. We take the projected distances of Fornax GCs from Mackey & Gilmore (2003), which we recalculate using a more recent distance estimate for Fornax of 147 ± 4 kpc (McConnachie 2012); this new distance is about 7 per cent larger than the 137 kpc used by Mackey & Gilmore. The updated GC distances are given in Table 1 and their radial distribution is shown in Fig. 9, where we also show the projected distance distribution predicted by our model for satellite and field dwarfs. Qualitatively, we find good agreement between observations and the simulations. To quantify the degree of agreement, we use the Kolmogorov-Smirnov (KS) test. The KS test returns a p-value, $p = 0.98$, when comparing the Fornax GCs with those of satellite analogues in the E-MOSAICS simulation, and a lower value, $p = 0.55$, when comparing with the field analogues. This indicates that any differences seen in Fig. 9 are consistent with random noise and thus not significant.

6 DISCUSSION

In this section we discuss in detail the implications of our results and what they can tell us about the formation history of the Fornax dSph.

6.1 The DM halo of the Fornax dSph

Our stellar-mass selected Fornax analogues are found in haloes of present-day mass, $M_{200} = 2.8^{+1.1}_{-1.0} \times 10^{10}$ M$_\odot$ (68 per cent confidence limit), and concentration, $c = 10.5^{+3.6}_{-2.6}$. These values apply to field galaxies, i.e. to Fornax-mass dwarfs that are central galaxies. The M_{200} and c values can be used to infer the halo scale radius, r_s, and characteristic density, ρ_0 (see Eq. 1). The resulting values of r_s and ρ_0 provide a good description also of the inner region ($r \lesssim r_s$) of our Fornax-mass satellites, as long as these satellites have not experienced stripping of their inner DM profile. This is because DM halo growth proceeds primarily by the deposition of newly accreted material in the outer parts of the halo with the inner parts remaining largely unchanged (Wang et al. 2011). Once a galaxy becomes a satellite, it stops accreting mass and, in fact, can lose mass by tidal stripping, with most of the decrease taking place at the outskirts of the halo while the inner region changes only slowly (e.g. Peñarrubia et al. 2008; Errani & Peñarrubia 2020). The profile of the inner halo changes appreciably only once a large fraction ($\gtrsim 50$ per cent) of the mass has been lost, and this will be manifest in changes in the orbits of stars and GCs (Peñarrubia et al. 2008; Fattahi et al. 2016). Thus, as long as the satellites have not suffered a large degree of tidal stripping, we expect that they should have similar inner DM profiles as their field counterparts (we explicitly show this for the halo scale radius, r_s, in Fig. 2).

We have found that the Fornax dSph has an atypically large number of GCs for its stellar mass. Observations have shown that the number and, in particular, the total mass in GCs correlates with halo mass (e.g. Forbes et al. 2018). The same correlation is well reproduced in the E-MOSAICS simulation (Bastian et al. 2020). This raises the question of whether we can take into account the richness of the Fornax GC system to better determine properties of its dark halo. We investigate this possibility in Appendix B, where we show that our Fornax analogues that have at least three GCs (the fraction of systems with at least five GCs is too low to obtain robust conclusions) reside in DM haloes that are, on average, 20 per cent more massive than the full Fornax-mass sample. Interestingly, the DM halo concentration does not show a trend with GC abundance.

Our average, our DM halo mass estimates are an order of magnitude larger than previous determinations based on the stellar kinematics of the Fornax dSph, which suggest a DM halo mass of few $\times 10^9$ M$_\odot$ (Goerdt et al. 2006; Boldrini et al. 2019; Meadows et al. 2020). However, our estimates are in good agreement with the recent non-parametric Jeans modelling of Read et al. (2019), who found a total mass of $\sim 2 \times 10^{10}$ M$_\odot$. The discrepancy could be due to the Fornax halo having experienced a large amount of tidal stripping, as suggested by Fattahi et al. (2016), Wang et al. (2017) and Genina et al. (2020). These studies used hydrodynamical simulations to select Fornax counterparts by matching the observed stellar velocity-dispersion and stellar half-mass radius in the first two of these papers and the stellar mass in the last one. If stripping is important then a $\sim 10^9$ M$_\odot$ halo is not representative of the halo in which the Fornax GCs formed and evolved for most of their lifetime before the galaxy fell into the Milky Way.

6.2 What determines the sinking time scale for GCs?

Our result agrees with earlier work that showed that in a cuspy DM halo, the orbits of GCs decay because of dynamical friction (e.g. Goerdt et al. 2006; Meadows et al. 2020). However, we estimate a longer decay time for the Fornax GCs that in previous work. The differences arise from two novel aspects introduced into this analysis. Firstly, we show that previous measurements of the Fornax DM halo based on simple stellar kinematic analyses give a mass that is too low (see discussion in Section 6.1); this leads to an estimate of the sinking timescale that is correspondingly too low (see Section 4). On average, the sinking timescale doubles in an $M_{200} = 3 \times 10^{10}$ M$_\odot$ halo compared to that in a halo of the previously assumed value of $M_{200} = 2 \times 10^9$ M$_\odot$.

Secondly, as pointed out in previous work, we know only the present-day positions of the GCs, not their birth positions (e.g. Angus & Diaferio 2009; Boldrini et al. 2019; Meadows et al. 2020). The sinking time increases rapidly with increasing distance, and even small changes in distance can have a considerable effect. To take this into account in our analysis, we used the GC positions and velocities at birth from the E-MOSAICS simulation which self-consistently models the formation and evolution of GCs in cuspy DM haloes. Our calculation shows that the majority (67 per cent) of GCs in Fornax-mass dwarfs survive to the present day and thus only a third are expected to sink to the centre of their galaxy in a Hubble time. The survival chance depends on the starting position of the GC: it is as low as 37 per cent for GCs formed within 1 kpc from the centre and as large as 92 per cent for GCs formed beyond 1 kpc from the centre.

6.3 Past and future orbits of the GCs in Fornax

Given the updated GC sinking times discussed in Section 6.2, we recalculate, in Fig. 10, the possible orbits of the Fornax GCs. The figure shows both the past (to the left of the vertical dotted line) and the future orbits assuming the median halo mass, $M_{200} = 3 \times 10^{10}$ M$_\odot$, and the median concentration, $c = 10$, of our Fornax analogue sample. The distances of GCs are in 3D and the orbit integration was done assuming circular orbits with present-day radii of $\sqrt{3/2}$ times their observed projected radial distance.

This simple model suggests that only one GC, Frn 4, was

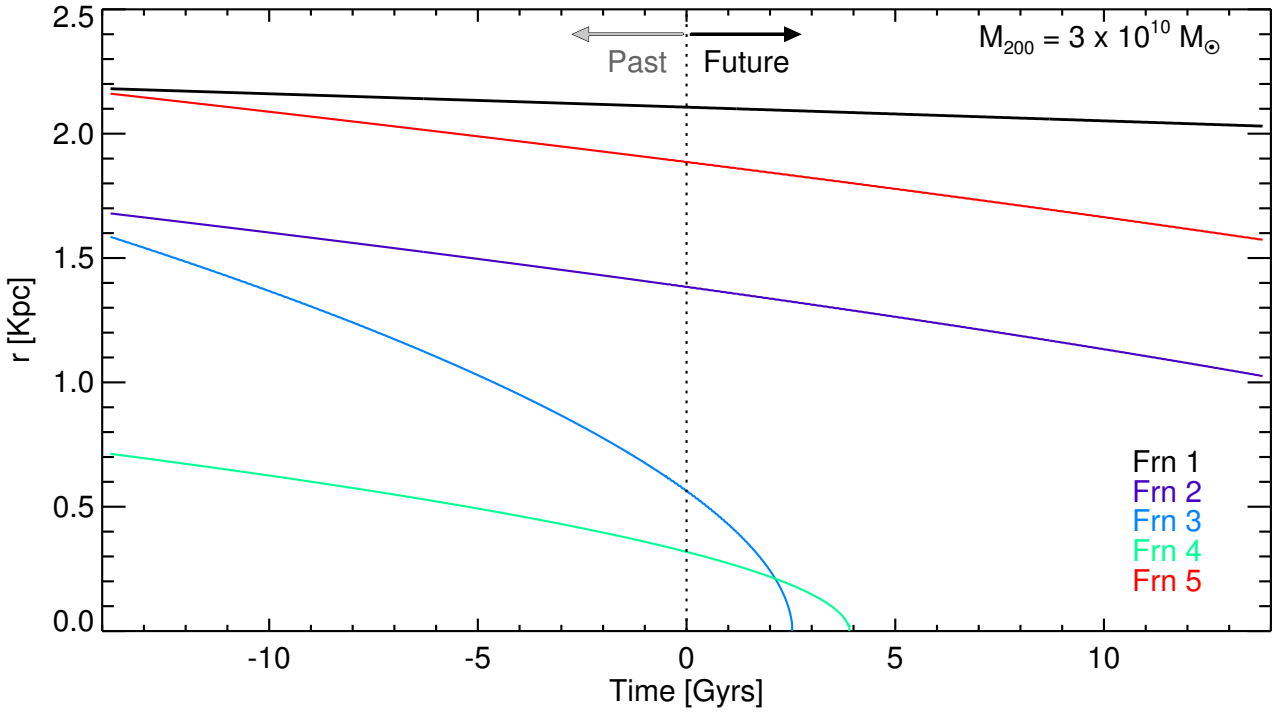

Figure 10. The orbital evolution of the GCs in Fornax assuming the median mass, $M_{200} = 3 \times 10^{10}$ M$_\odot$, and the median concentration, $c = 10$, for the DM halo of Fornax's. Negative time values correspond to past orbits and positive ones to future orbits. Each colour corresponds to one of the 5 GCs in Fornax (see bottom-right legend). In the past the GCs were farther from the galaxy centre, especially Fornax 3, which is the most massive, and Fornax 4, which today is the closest to the centre.

born at a small radial distance, $r_{\rm init} = 700$ pc, which is approximately the half-light radius of the present-day Fornax (as given by McConnachie 2012). For the remaining four GCs, the initial distances are larger than 1.5 kpc, which suggests that at least some of them were accreted (see also Boldrini et al. 2020). This result is in good agreement with our model prediction that around half of the present-day surviving GCs are of accreted origin. The sinking time varies from GC to GC depending on the initial distances and masses; Frn 1, Frn 2, and Frn 5 could still survive for another Hubble time mainly because of their large initial distances. Interestingly, the time for Frn 3 to sink is the shortest amongst the five even though it started from $r_{\rm init} = 1.5$ kpc, which is twice as far as Frn 4. This is due to the fact that Frn 3 is the most massive GC of the five, with a mass, $M_\star = 5 \times 10^5$ M$_\odot$.

We note that the orbital evolution in Fig. 10 is highly simplified and does not take into account that the GCs are likely to be on eccentric orbits. For example, E-MOSAICS predicts that at birth the GCs in Fornax-mass dwarfs have an orbital ellipticity of $0.64^{+0.20}_{-0.28}$ (68th per centile). Furthermore, there is indirect evidence that the Fornax dSph might have had a major merger $\sim$10 Gyrs ago (Yozin & Bekki 2012; Benítez-Llambay et al. 2016) and that it is potentially undergoing severe tidal stripping (Wang et al. 2017; Genina et al. 2020). The latter process, if it takes place rapidly enough, could lead to the dissolution of the GC system in the outskirts of the Milky Way halo before Frn 3 can sink to the centre.

6.4 GCs and the core-cusp problem

The existence of GCs close to the centre of Fornax has often been adduced as evidence that this galaxy's DM halo has a constant density core. Here we have shown, to the contrary, that cuspy DM haloes with galaxies of simliar stellar mass to Fornax are expected to have a similar GC radial distribution: the GCs in Fornax cannot be used to rule out a cuspy halo (see also Angus & Diaferio 2009; Meadows et al. 2020). In fact, the absence of an extended core, of radius $\sim$ 1 kpc, in Fornax is supported by other probes. Read et al. (2019) used higher-order moments of the velocity distribution to break the degeneracy between mass and velocity anisotropy and found that the stellar kinematics in Fornax favour an increase of an order of magnitude in DM density between radii of 1 and 0.1 kpc, with a core, if present, having a radius $\lesssim 0.2$ kpc. Such a core radius is too small to lead to a stalling of the orbital decay of GCs, which takes place at around $\sim 1/3$ of the core radius (Meadows et al. 2020).

Our model predicts that a third of the GCs associated with Fornax-mass dwarfs have sunk to the centre of their host galaxies where they may have been tidally disrupted. It remains to be seen what is the corresponding fraction of destroyed GCs if the DM profile had a core, but it is likely lower. Thus, identifying in observations the fraction of GCs that were destroyed is, in principle, a promising avenue for distinguishing between a cusp and a core in Fornax. The extent of tidal stripping experienced by GC is sensitive to the central DM density profile: in cuspy haloes GCs are more extended and have lower mass loss that in haloes with cores (e.g. Amorisco 2017; Webb & Vesperini 2018; Orkney et al. 2019) but it is unclear if this difference can be used as a test of the inner structure of the halo.

7 CONCLUSIONS

We have investigated the number and radial distribution of GCs in the Fornax dSph with the goal of testing whether the GC population in this galaxy is consistent with a cuspy halo, the simplest prediction of the ΛCDM cosmological model (Navarro et al. 1996b, 1997). Our study has been motivated in part by the ongoing debate on whether the Fornax GCs are a robust signature of a kiloparsec-sized core at the centre of this galaxy's halo (e.g. see discussion in Meadows et al. 2020). To this end we have analyzed the E-MOSAICS simulation (Pfeffer et al. 2018; Kruijssen et al. 2019a), which includes a subgrid prescription for self-consistently following galaxy and GC formation and evolution within the EAGLE cosmological hydrodynamics framework (Schaye et al. 2015; Crain et al. 2015).

We have proceeded by identifying a sample of Fornax analogues, selected to have a similar stellar mass, within a factor of two, as the Fornax dSph, i.e. in the range $[2, 8] \times 10^7\,\mathrm{M}_\odot$. E-MOSAICS is well suited for this study because it contains a large sample (1154) of Fornax-mass dwarfs, within which GC formation and evolution is followed in a full cosmological context. To account for the GC orbital decay due to dynamical friction, we have post-processed the orbits of GCs starting from their initial positions as determined by E-MOSAICS, and assuming that they evolve in the NFW profile that best fits each host halo in the simulation. The initial conditions are given by the GC positions and velocities at birth for *in situ* GCs, and at infall for accreted GCs. We applied a tides model to account for the disruption of GC by their host halo. We then investigated the number and radial distribution of GCs of stellar mass, $M_\star \geq 4 \times 10^4\,\mathrm{M}_\odot$, corresponding to the smallest of the five well-studied GCs in Fornax. Our main conclusions may be summarised as follows:

(i) Field Fornax-mass dwarfs reside in haloes of median mass, $M_{200} \approx 2.8 \times 10^{10}\,\mathrm{M}_\odot$, and concentration, $c \approx 10$ (see Fig. 1).

(ii) The population of GCs of Fornax analogues consists, in nearly equal amounts, of *in situ* (45 per cent) and accreted objects (55 per cent).

(iii) The GCs of Fornax are typically old, with a median age, $t_{\mathrm{age}} \approx 12$ Gyrs. The fraction of GCs younger than 12 Gyrs is 77 per cent for *in situ* GCs and 23 per cent for accreted GCs. This is because *in situ* GCs, which form close to their host centre, are more likely to be destroyed, while the accreted GCs started orbital decay at larger initial distances (see Fig. 3).

(iv) Orbital decay leads to 33 per cent of GCs sinking to the centre where they can be tidally disrupted in a cuspy halo (see Fig. 6).

(v) Most of the Fornax-mass dwarfs have one (≈ 30 per cent) or no (≈ 35 per cent) GCs, with very few having several. The results are similar for both satellite and field dwarfs (see Fig. 5).

(vi) The median radial distance of surviving GCs is 1.7 kpc, with 10 and 90 percentiles of 0.3 and 8.5 kpc respectively (see Fig. 6).

(vii) Satellite galaxies have more concentrated GC distributions than their field analogues. *In situ* GCs are also more radially concentrated than their accreted counterparts (see Fig. 8).

Our model predicts that only a small fraction (3 per cent) of Fornax-mass dwarfs have at least as many GCs as are observed in Fornax. This result does not pose a challenge to our model since observations similarly show that Fornax has a surprisingly large number of GCs for its stellar mass (e.g. see Figure C1 in Forbes et al. 2018). In fact, most observed dwarfs with similar masses to Fornax have, at most, only one or two GCs, in agreement with our model predictions.

The observed radial distribution of the GCs in Fornax agrees very well with our model prediction for satellite Fornax analogues (KS test p-value of 0.98). This indicates that, contrary to previous claims, the distribution of GCs in Fornax can be reproduced in a DM halo that has a central cusp. Furthermore, our model predicts that the $z = 0$ surviving GCs represent ≈ 67 per cent of the GCs ever associated with Fornax, ie. born within, or accreted onto, Fornax and thus suggests that Fornax may have had an additional ∼2 GCs that sunk to its centre and could have been destroyed. One such candidate has recently been discovered: a low mass GC ∼30 pc away in projection from the centre of Fornax which has an irregular shape that could indicate that it is undergoing tidal disruption (Wang et al. 2019).

By modelling GC formation and evolution in a cuspy DM halo, our work has demonstrated that the Fornax GC system cannot be used to rule out a central cusp in this galaxy's halo. The next steps involve investigating if the number and radial distribution of GCs differs between DM haloes with cusps and cores. One way to do so would be to run E-MOSAICS with an increased star formation gas density threshold, which has been shown to lead to the formation of cores within the EAGLE galaxy formation model (Benítez-Llambay et al. 2019). Such a simulation would predict the GC distribution for profiles with cores and, by comparing directly against our results, would help identify which GC statistics are best suited to distinguish between a central core or cusp in the DM profile.

ACKNOWLEDGEMENTS

SS and CSF were supported by the European Research Council through ERC Advanced Investigator grant, DMIDAS [GA 786910], to CSF and by the Science and Technology Facilities Council (STFC) [grant number ST/F001166/1, ST/I00162X/1, ST/P000541/1]. MC acknowledges support by the EU Horizon 2020 research and innovation programme under a Marie Skłodowska-Curie grant agreement 794474 (DancingGalaxies). MRC acknowledges financial support from a CITA National Fellowship. AD and RAC are supported by Royal Society University Research Fellowships. JP gratefully acknowledges funding from a European Research Council consolidator grant (ERC-CoG-646928-Multi-Pop). MRC and JMDK gratefully acknowledge funding from the European Research Council (ERC) under the European Union's Horizon 2020 research and innovation programme via the ERC Starting Grant MUSTANG (grant agreement number 714907). JMDK gratefully acknowledges funding from the Deutsche Forschungsgemeinschaft (DFG, German Research Foundation) through an Emmy Noether Research Group (grant number KR4801/1-1) and the DFG Sachbeihilfe (grant number KR4801/2-1). This work used the DiRAC Data Centric system at Durham University, operated by ICC on behalf of the STFC DiRAC HPC Facility (www.dirac.ac.uk). This equipment was funded by BIS National E-infrastructure capital grant ST/K00042X/1, STFC capital grant ST/H008519/1, and STFC DiRAC Operations grant ST/K003267/1 and Durham University. DiRAC is part of the National E-Infrastructure.

DATA AVAILABILITY

The used and data produced in this paper are available upon reasonable request to the corresponding author.

REFERENCES

Amorisco N. C., 2017, ApJ, 844, 64
Amorisco N. C., Agnello A., Evans N. W., 2013, MNRAS, 429, L89
Angulo R. E., Lacey C. G., Baugh C. M., Frenk C. S., 2009, MNRAS, 399, 983
Angus G. W., Diaferio A., 2009, MNRAS, 396, 887
Bastian N., 2008, MNRAS, 390, 759
Bastian N., Pfeffer J., Kruijssen J. M. D., Crain R. A., Trujillo-Gomez S., Reina-Campos M., 2020, preprint, (arXiv:2005.05991)
Battaglia G., et al., 2006, A&A, 459, 423
Battaglia G., Helmi A., Tolstoy E., Irwin M., Hill V., Jablonka P., 2008, ApJ, 681, L13
Benítez-Llambay A., Navarro J. F., Abadi M. G., Gottlöber S., Yepes G., Hoffman Y., Steinmetz M., 2016, MNRAS, 456, 1185
Benítez-Llambay A., Frenk C. S., Ludlow A. D., Navarro J. F., 2019, MNRAS, 488, 2387
Binney J., Tremaine S., 2008, Galactic Dynamics: Second Edition. Princeton University Press
Boldrini P., Mohayaee R., Silk J., 2019, MNRAS, 485, 2546
Boldrini P., Mohayaee R., Silk J., 2020, MNRAS, 492, 3169
Booth C. M., Schaye J., 2009, MNRAS, 398, 53
Bose S., et al., 2019, MNRAS, 486, 4790
Cole D. R., Dehnen W., Read J. I., Wilkinson M. I., 2012, MNRAS, 426, 601
Crain R. A., et al., 2015, MNRAS, 450, 1937
Dalla Vecchia C., Schaye J., 2012, MNRAS, 426, 140
Davis M., Efstathiou G., Frenk C. S., White S. D. M., 1985, ApJ, 292, 371
Deason A., Wetzel A., Garrison-Kimmel S., 2014, ApJ, 794, 115
Di Cintio A., Brook C. B., Macciò A. V., Stinson G. S., Knebe A., Dutton A. A., Wadsley J., 2014, MNRAS, 437, 415
Dolag K., Borgani S., Murante G., Springel V., 2009, MNRAS, 399, 497
Errani R., Peñarrubia J., 2020, MNRAS, 491, 4591
Fattahi A., et al., 2016, MNRAS, 457, 844
Flores R. A., Primack J. R., 1994, ApJ, 427, L1
Forbes D. A., Read J. I., Gieles M., Collins M. L. M., 2018, MNRAS, 481, 5592
Genina A., et al., 2018, MNRAS, 474, 1398
Genina A., et al., 2019a, preprint, (arXiv:1911.09124)
Genina A., Frenk C. S., Benítez-Llambay A. r., Cole S., Navarro J. F., Oman K. A., Fattahi A., 2019b, MNRAS, 488, 2312
Genina A., Read J. I., Fattahi A., Frenk C. S., 2020, preprint, p. arXiv:2011.09482 (arXiv:2011.09482)
Gilmore G., Wilkinson M. I., Wyse R. F. G., Kleyna J. T., Koch A., Evans N. W., Grebel E. K., 2007, ApJ, 663, 948
Goerdt T., Moore B., Read J. I., Stadel J., Zemp M., 2006, MNRAS, 368, 1073
Harris W. E., Blakeslee J. P., Harris G. L. H., 2017, ApJ, 836, 67
Hellwing W. A., Frenk C. S., Cautun M., Bose S., Helly J., Jenkins A., Sawala T., Cytowski M., 2016, MNRAS, 457, 3492
Hernandez X., Gilmore G., 1998, MNRAS, 297, 517
Hopkins P. F., 2013, MNRAS, 428, 2840
Hughes M. E., Pfeffer J., Martig M., Bastian N., Crain R. A., Kruijssen J. M. D., Reina-Campos M., 2019, MNRAS, 482, 2795
Hughes M. E., Pfeffer J. L., Martig M., Reina-Campos M., Bastian N., Crain R. A., Kruijssen J. M. D., 2020, MNRAS, 491, 4012
Inoue S., 2009, MNRAS, 397, 709
Kaplinghat M., Tulin S., Yu H.-B., 2016, Phys. Rev. Lett., 116, 041302
Kaur K., Sridhar S., 2018, ApJ, 868, 134
Kruijssen J. M. D., 2012, MNRAS, 426, 3008
Kruijssen J. M. D., Pelupessy F. I., Lamers H. J. G. L. M., Portegies Zwart S. F., Icke V., 2011, MNRAS, 414, 1339
Kruijssen J. M. D., Pfeffer J. L., Crain R. A., Bastian N., 2019a, MNRAS, 486, 3134
Kruijssen J. M. D., Pfeffer J. L., Reina-Campos M., Crain R. A., Bastian N., 2019b, MNRAS, 486, 3180
Kruijssen J. M. D., et al., 2020, preprint, (arXiv:2003.01119)
Law D. R., Majewski S. R., 2010, ApJ, 714, 229
Mackey A. D., Gilmore G. F., 2003, MNRAS, 340, 175
Malhan K., Valluri M., Freese K., 2020, preprint, (arXiv:2005.12919)
McConnachie A. W., 2012, AJ, 144, 4
Meadows N., Navarro J. F., Santos-Santos I., Benítez-Llambay A., Frenk C., 2020, MNRAS, 491, 3336
Moore B., 1994, Nature, 370, 629
Moster B. P., Naab T., White S. D. M., 2013, MNRAS, 428, 3121
Navarro J. F., Eke V. R., Frenk C. S., 1996a, MNRAS, 283, L72
Navarro J. F., Frenk C. S., White S. D. M., 1996b, ApJ, 462, 563
Navarro J. F., Frenk C. S., White S. D. M., 1997, ApJ, 490, 493
Oñorbe J., Boylan-Kolchin M., Bullock J. S., Hopkins P. F., Kereš D., Faucher-Giguère C.-A., Quataert E., Murray N., 2015, MNRAS, 454, 2092
Oman K. A., Marasco A., Navarro J. F., Frenk C. S., Schaye J., Benítez-Llambay A. r., 2019, MNRAS, 482, 821
Orkney M. D. A., Read J. I., Petts J. A., Gieles M., 2019, preprint, (arXiv:1906.04759)
Pascale R., Posti L., Nipoti C., Binney J., 2018, MNRAS, 480, 927
Peñarrubia J., Navarro J. F., McConnachie A. W., 2008, ApJ, 673, 226
Petts J. A., Gualandris A., Read J. I., 2015, MNRAS, 454, 3778
Pfeffer J., Kruijssen J. M. D., Crain R. A., Bastian N., 2018, MNRAS, 475, 4309
Pfeffer J. L., Trujillo-Gomez S., Kruijssen J. M. D., Crain R. A., Hughes M. E., Reina-Campos M., Bastian N., 2020, MNRAS, 499, 4863
Planck Collaboration XVI 2014, A&A, 571, A16
Pontzen A., Governato F., 2012, MNRAS, 421, 3464
Read J. I., Gilmore G., 2005, MNRAS, 356, 107
Read J. I., Goerdt T., Moore B., Pontzen A. P., Stadel J., Lake G., 2006, MNRAS, 373, 1451
Read J. I., Walker M. G., Steger P., 2019, MNRAS, 484, 1401
Reina-Campos M., Kruijssen J. M. D., 2017, MNRAS, 469, 1282
Reina-Campos M., Kruijssen J. M. D., Pfeffer J. L., Bastian N., Crain R. A., 2019, MNRAS, 486, 5838
Reina-Campos M., Hughes M. E., Kruijssen J. M. D., Pfeffer J. L., Bastian N., Crain R. A., Koch A., Grebel E. K., 2020, MNRAS, 493, 3422
Renaud F., Gieles M., Boily C. M., 2011, MNRAS, 418, 759
Rocha M., Peter A. H. G., Bullock J. S., Kaplinghat M., Garrison-Kimmel S., Oñorbe J., Moustakas L. A., 2013, MNRAS, 430, 81
Sawala T., et al., 2015, MNRAS, 448, 2941
Schaller M., Dalla Vecchia C., Schaye J., Bower R. G., Theuns T., Crain R. A., Furlong M., McCarthy I. G., 2015, MNRAS, 454, 2277
Schaye J., et al., 2015, MNRAS, 446, 521
Schechter P., 1976, ApJ, 203, 297
Schneider A., Trujillo-Gomez S., Papastergis E., Reed D. S., Lake G., 2017, MNRAS, 470, 1542
Shao S., Gao L., Theuns T., Frenk C. S., 2013, MNRAS, 430, 2346
Shao S., Cautun M., Deason A. J., Frenk C. S., Theuns T., 2018, MNRAS, 479, 284
Spergel D. N., Steinhardt P. J., 2000, Phys. Rev. Lett., 84, 3760
Springel V., 2005, MNRAS, 364, 1105
Springel V., Yoshida N., White S. D. M., 2001, New Astron, 6, 79
Springel V., Di Matteo T., Hernquist L., 2005, MNRAS, 361, 776
Strigari L. E., Frenk C. S., White S. D. M., 2010, MNRAS, 408, 2364
Strigari L. E., Frenk C. S., White S. D. M., 2017, ApJ, 838, 123
Tremaine S. D., Ostriker J. P., Spitzer L. J., 1975, ApJ, 196, 407
Trujillo-Gomez S., Kruijssen J. M. D., Reina-Campos M., Pfeffer J. L., Keller B. W., Crain R. A., Bastian N., Hughes M. E., 2020, preprint, p. arXiv:2005.02401 (arXiv:2005.02401)
Usher C., Pfeffer J., Bastian N., Kruijssen J. M. D., Crain R. A., Reina-Campos M., 2018, MNRAS, 480, 3279
Walker M. G., Peñarrubia J., 2011, ApJ, 742, 20

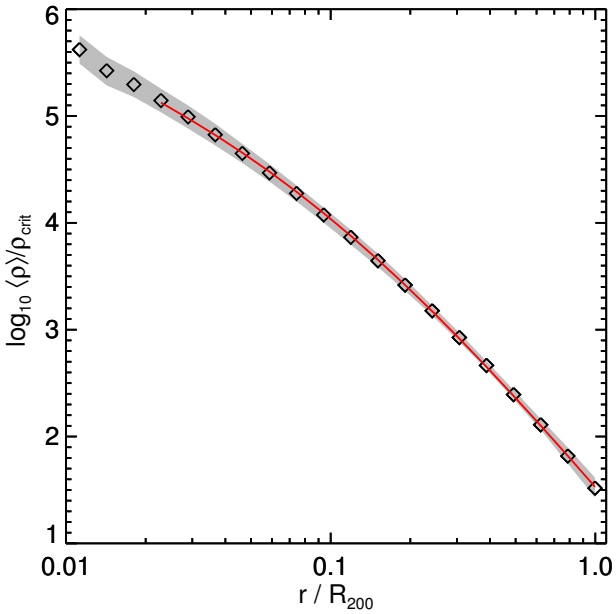

Figure A1. Mean, radially averaged density profile, $\rho(r)$, for the field Fornax-mass haloes in the simulation. The red line shows the best-fit NFW profile.

Walker M. G., Mateo M., Olszewski E. W., Peñarrubia J., Evans N. W., Gilmore G., 2009, ApJ, 704, 1274
Wang J., et al., 2011, MNRAS, 413, 1373
Wang M. Y., et al., 2017, MNRAS, 468, 4887
Wang M.-Y., et al., 2018, preprint, p. arXiv:1809.07801 (arXiv:1809.07801)
Wang M. Y., et al., 2019, ApJ, 875, L13
Webb J. J., Vesperini E., 2018, MNRAS, 479, 3708
Wiersma R. P. C., Schaye J., Smith B. D., 2009, MNRAS, 393, 99
Yozin C., Bekki K., 2012, ApJ, 756, L18
de Boer T. J. L., Fraser M., 2016, A&A, 590, A35
de Boer T. J. L., et al., 2012, A&A, 544, A73

APPENDIX A: THE DM DENSITY PROFILE OF FORNAX-MASS DWARFS

In agreement with previous results from Eagle (Schaller et al. 2015), the spherically averaged density profiles of our Fornax-mass haloes are well fit by the NFW profile. This is shown in Fig. A1.

APPENDIX B: THE HALO PROPERTIES OF GC RICH DWARFS

In Fig. B1 we show how the mass and concentration of the field Fornax analogues varies when, in addition to selecting the analogues according to stellar mass, we also require that they have a large number of GCs. To obtain a reasonable sample of dwarfs with many GCs, we select the subsample that has three or more GCs. The left-hand panel of Fig. B1 shows the PDF of M_{200} for all the field dwarfs (dotted line) that were part of our initial, stellar-mass only selection and field dwarfs that have three or more GCs (solid line). The latter reside in slightly more massive haloes, with a median, $M_{200} = 3.4 \times 10^{10}$ M$_\odot$, that is 1.2 times larger than the median of the full Fornax-analogue sample. This agrees with the fact that more massive galaxies host more GCs (e.g. Harris et al. 2017). The

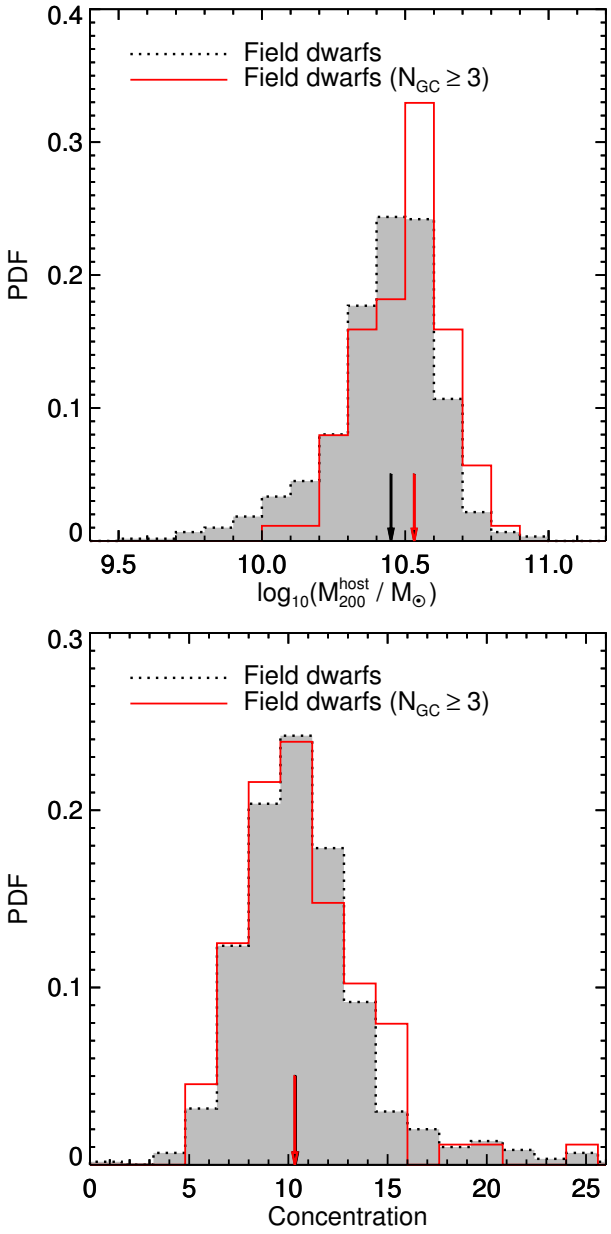

Figure B1. Comparison of the mass and concentration of DM haloes of two Fornax-analogue populations. The black dotted line shows the distribution for our reference population of all Fornax-mass dwarfs. The red solid line shows the subset of systems that have 3 or more GCs. The vertical arrows indicate the median of each PDF.

difference in the concentrations between the two samples is rather small, as shown in the right-hand panel.

APPENDIX C: THE MASS EVOLUTION OF GCS IN FORNAX-MASS DWARFS

In Section 4 we discussed the effect of GC mass on the decay of its orbit. To make our predictions as realistic as possible, we accounted for the decrease in GC mass as a function of time. The average trend, quantified as the ratio of the GC mass at time t and the initial mass, as a function of the GC age, obtained from E-MOSAICS, is shown in Fig. C1. As described in Section 2,

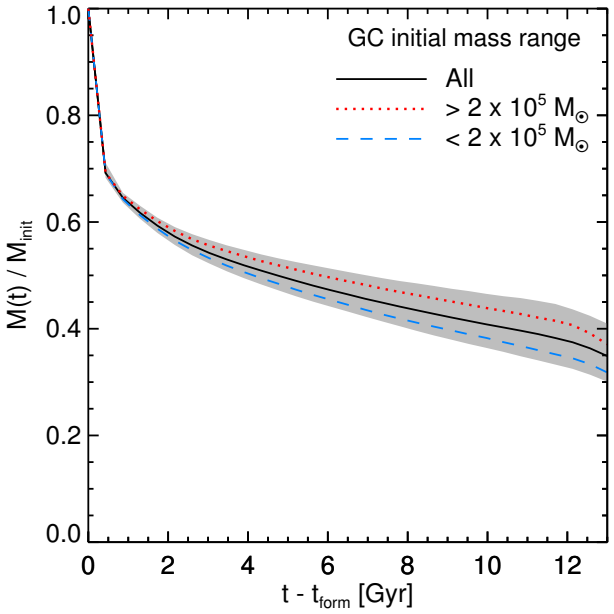

Figure C1. The average mass evolution of our GC sample. The plot shows the ratio of the mass at a given time to the initial GC mass as a function of the time since the GC formed. The result for all the GCs is shown by the black solid line with the shaded region showing the 68 percentile object-to-object scatter. The various coloured lines show the results for GCs in different initial mass ranges (see legend). Each of the GC subsamples contains roughly half of the full sample.

E-MOSAICS accounts for the GC mass lost by stellar evolution, two-body relaxation and tidal shocks. When calculating dynamical friction in post-processing, we assumed that the GC mass follows the relation shown in the figure (solid black line). The mass evolution is slightly affected by the initial mass of the GCs but, for simplicity, we neglect this effect.